Published in final edited form as:

Nature. 2016 July 7; 535(7610): 178–181. doi:10.1038/nature18316.

The Nature of Mutations Induced by Replication-Transcription Collisions

T. Sabari Sankar[1,2,*], **Brigitta D. Wastuwidyaningtyas**[2,*], **Yuexin Dong**[1], **Sarah A. Lewis**[2], and **Jue D. Wang**[1,2,†]

[1]Department of Bacteriology, University of Wisconsin-Madison, Madison, WI 53706

[2]Department of Molecular and Human Genetics, Baylor College of Medicine, Houston, TX 77030

Summary

The DNA replication and transcription machineries share a common DNA template and thus can collide with each other co-directionally or head-on[1,2]. Replication-transcription collisions can cause replication fork arrest, premature transcription termination, DNA breaks, and recombination intermediates threatening genome integrity[1–10]. Collisions may also trigger mutations, which are major contributors of genetic disease and evolution[5,7,11]. However, the nature and mechanisms of collision-induced mutagenesis remain poorly understood. Here we reveal the genetic consequence of replication-transcription collisions in actively dividing bacteria to be two classes of mutations: duplications/deletions and base substitutions in promoters. Both signatures are highly deleterious but are distinct from the well-characterized base substitutions in coding sequence. Duplications/deletions are likely caused by replication stalling events that are triggered by collisions; their distribution patterns are consistent with where the fork first encounters a transcription complex upon entering a transcription unit. Promoter substitutions result mostly from head-on collisions and frequently occur at a nucleotide conserved in promoters recognized by the major sigma factor in bacteria. This substitution is generated via adenine deamination on the template strand in the promoter open complex, as a consequence of head-on replication perturbing transcription initiation. We conclude that replication-transcription collisions induce distinct mutation signatures by antagonizing replication and transcription, not only in coding sequences but also in gene regulatory elements.

†Correspondence and requests for materials should be addressed to J.D.W (wang@bact.wisc.edu).
*These authors contributed equally

Author Contributions:

J.D.W. conceptualized the study. T.S.S., B.D.W. and J.D.W. designed the experiments. T.S.S. performed *thyP3* fluctuation tests and sequencing of *recA*, *yqjH*, *mutSL*, *adeC* mutants, comparative genomic analyses, nitrous acid mutagenesis, competition assays and plating efficiency of mutants. B.D.W. developed the forward mutation assay, fluctuation tests and sequencing of wild-type strains, qRT-PCR, nalidixic acid fluctuation test, doubling time measurements and developed the restriction digest screening. Y.D. assisted the competition assay, plating efficiency and *mutSL* fluctuation tests. S.A.L. performed *thyP3* fluctuation tests with B.D.W. T.S.S., B.D.W. and J.D.W. analyzed the data and wrote the manuscript.

The authors declare no competing financial interests.

Readers are welcome to comment on the online version of this article at www.nature.com/nature.

Mutations cause genetic diseases and drive evolution by altering either the gene coding sequence or the noncoding elements that control gene expression. A variety of mechanisms underlie mutagenesis: DNA replication errors, error-prone repair, transcription-associated mutagenesis (TAM), and replication stalling-mediated template switch[10,12–15]. Many mutagenic mechanisms depend on two fundamental processes- replication or transcription. However, little is known about mutagenic mechanisms involving replication-transcription collision, an unavoidable outcome of the two processes sharing the same DNA template. Identifying the mutagenic consequences of replication-transcription collisions remains an important challenge due to the difficulty of differentiating collision-induced mutation events from that of either replication or transcription.

An experimental approach to identify collision-induced mutagenesis is to analyze the mutagenic consequence of altering the relative directionality of transcription to replication[7,10–12]. Head-on collisions are proposed to generate mutations more frequently than co-directional collisions, which may underlie the genome-wide bias for essential genes to be transcribed co-directional to replication[5,7,11]. In support of this hypothesis, in the bacterium *Bacillus subtilis* in which 94% of essential genes are co-directional[16], base substitution rates are higher within genes oriented head-on than co-directional to replication[7,11]. However, the orientation-dependent difference in substitution rates can also be explained by the difference in the fidelity between leading and lagging strand replication[12,15,17,18], challenging the notion that collisions generate base substitutions in coding sequence[11,19]. Thus, conclusive evidence for collision-induced mutations is still lacking and necessitates a systematic analysis of collision-generated mutation signatures beyond base substitutions in coding sequence.

Here, we investigate whether mutations are generated by collisions by identifying the signatures and characterizing mechanisms of mutations caused by co-directional versus head-on collisions. We first developed an assay that can detect a wide range of mutations in *B. subtilis*. We chose the thymidylate synthetase gene *thyP3* because any complete loss-of-function mutation in *thyP3* can be selected using trimethoprim resistance (Extended Data Fig. 1a). To evaluate the effect of gene directionality on mutagenesis, we placed *thyP3* under an IPTG-inducible promoter at a single location on the chromosome in either co-directional or head-on orientation (Fig. 1a). To estimate mutation rates, we performed the Luria-Delbrück fluctuation test using multiple growth cultures, selected for *thyP3* mutants after growth, and statistically determined the rate of spontaneous mutations in *thyP3* (Fig. 1b)[20,21]. Two additional features of our assay allowed critical analyses of mutagenesis. First, we chose the nonnative, phage-encoded *thyP3* as the target sequence and deleted *thyA*, the native homolog of *thyP3*. We avoided using a native gene to evaluate the impact of gene directionality on mutagenesis because evolution may have already eliminated potential mutation hotspots within a native gene in its original orientation. Second, we took advantage of the temperature sensitivity of a second endogenous gene, *thyB*, to ensure that mutants were not defective during growth, which could alter the apparent mutation rate. We grew cells at the permissive temperature (37 °C), during which the functional ThyB masks any competitive disadvantage of *thyP3* mutations (Extended Data Fig. 1b). Selection was done at a non-permissive temperature under which ThyB is inactivated and phenotypes associated with *thyP3* mutation would be exposed (Fig. 1b, and Extended Data Fig. 1c). In the presence

of *thyB*, mutants follow the Luria-Delbrück distribution (Fig. 1c), demonstrating that mutations arise with constant rate per cell division, before and not after selection[20,21]. Notably, the use of *thyB* was critical because without *thyB*, mutants followed the Poisson distribution instead of the expected Luria-Delbrück distribution (Fig. 1c), presumably due to the growth defect of *thyP3* mutants (Extended Data Fig. 1d).

Using this assay, we compared mutations resulting from co-directional versus head-on oriented *thyP3*. When induced by IPTG, transcription reaches similar levels from either co-directional or head-on *thyP3* (Extended Data Fig. 2a). A ~60% increase of total mutation rate in the head-on *thyP3* compared to co-directional *thyP3* was observed (Fig. 1d and Extended Data Fig. 2b–e). Next, we sequenced ~2000 mutants and obtained ~400 distinct mutations (Extended Data Fig. 3–4). Only less than a third of mutations observed in *thyP3* under induced transcription were base substitutions within the coding region. The remaining majority of mutations fall into two prominent classes: indels (insertions/deletions) and promoter base substitutions. Their mutation rates are strongly and differentially altered by transcription directionality and strength (Extended Data Fig. 2e). These alterations are mostly not due to competitive or selection bias of the mutants (Extended Data Fig. 5). Further analyses, described below, revealed that indels and promoter substitutions are likely induced by replication-transcription collisions.

Indels are likely generated upon stalling of a replication fork after collision with a transcription complex or a transcription factor[3,22]. First, the majority of indels are duplications/deletions between repeated DNA sequences (3–522 bp, Extended Data Fig. 6a), which were proposed to originate from slippage/template switch of stalled replication forks[13,14]. Second, the frequencies of indels at different locations within *thyP3* are strongly influenced by its transcription orientation and strength (Fig. 2a–f, Extended Data Fig. 6b). When *thyP3* was co-directional to replication, indels were predominantly enriched at the promoter and 5′ half of the coding region (Fig. 2a), including promoter-proximal regions where RNA polymerases (RNAP) are known to often pause[8]. In contrast, when *thyP3* was head-on, indels were found predominantly within the 3′ half (Fig. 2b), a bias that is largely absent when transcription was un-induced (at basal level) (Fig. 2c, d). This transcription-dependent enrichment pattern reflects the vicinity where the replication fork first encounters a transcription complex upon entering a transcription unit (Fig 2g, Extended Data Fig. 6c). Promoter deletions depended on the recombination protein RecA, thus are mostly caused by recombination[13] after replication fork collision with transcription initiation complex[22] or repressors[23] (Extended Data Fig. 7). However, the distribution of indels within the transcribed sequence was not affected by RecA, suggesting that recombination is not necessary for their generation. Instead, collision with transcription elongation complex[3,8,24] stalls replication fork progression, which can induce fork slippage, template switch or fork reversal that leads to duplications/deletions, or by collision-generated DNA breaks[6–9] followed by microhomology-mediated break-induced replication (MMBIR) or microhomology-mediated end joining (MMEJ) (Extended Data Fig. 6e,f)[14]. Our work thus reveals the strong contribution of replication-transcription conflicts to the generation of indels.

We next analyzed base substitutions in the coding sequence, which have been proposed to be generated by replication-transcription conflicts[11]. In contrast to indels, base substitutions within coding sequence were not enriched near locations of replication-transcription collisions (Fig. 3a–d). Base substitution rates were not higher under induced transcription compared to basal levels when considering identical mutation target sites (Extended Data Fig. 8a). We again observed higher substitution rates in coding sequence of head-on than co-directional genes[7,11], which are most likely due to different replication fidelity between leading and lagging strands[12,18], although collisions cannot be ruled out as a source of these mutations.

In contrast to coding sequence substitutions, promoter base substitutions were elevated upon induction of transcription, suggesting that transcription initiation causes genome instability at the promoter (Fig. 3e, Extended Data Fig. 8b). Most strikingly, this increase in promoter substitution rates is much stronger (400%) for head-on than co-directional transcription, strongly suggesting that head-on collisions generate promoter substitutions. To examine the generality of this observation, we performed a genome-wide phylogenetic analysis to estimate the number of nucleotide substitutions in promoters from multiple strains of *Bacillus*. The analysis showed that promoters of head-on genes have higher nucleotide substitutions than promoters of co-directional genes (Fig. 3f). Thus, head-on transcription not only increases mutation rate of the promoter sequence specifically studied above, but on a genome-wide scale in natural populations.

The most frequent substitution within the *thyP3* promoter is at a conserved nucleotide in the −10 element recognized by the major sigma factor, T_{-7} (Fig. 4a). $T_{-7}\rightarrow C_{-7}$ substitution accounted for all promoter substitutions and 50% of total mutation events upon induced transcription of head-on *thyP3* (Fig. 3e). This enrichment is not due to competitive advantage of C_{-7} mutant over wild-type or other *thyP3* mutants (Fig. 4b, Extended Data Fig. 5a–c), supporting $T_{-7}\rightarrow C_{-7}$ as a bona fide mutation hotspot obtainable with our assay. Importantly, T_{-7} is conserved across species and occurs in promoters of ~50–70% of essential genes in *B. subtilis* and *E. coli*[25]. The possibility that these promoters are all susceptible to collision-induced T→C mutagenesis implicates a previously unidentified, pervasive mechanism that can inactivate transcription of many genes and result in loss of viability. Indeed, in *E. coli* $T_{-7}\rightarrow C_{-7}$ was observed as a mutation hotspot in the head-on orientation in a plasmid-based assay (Extended Data Fig. 8d)[26] and T→C was also observed in other positions of *cis*-regulatory elements beyond −7 position[27], suggesting that base substitutions in gene-regulatory elements is a signature of head-on transcription in bacteria.

To examine the mechanism underlying this mutation, we used a restriction enzyme-based assay that exclusively detects $T_{-7}\rightarrow C_{-7}$ (Extended Data Fig. 8e) in *thyP3* to test several alternatives. First, we found that the error prone DNA polymerase PolIV, which was proposed to be responsible for collision-induced substitutions[19], is not a major contributor of this mutation (Fig. 4c). Second, $T_{-7}\rightarrow C_{-7}$ is not generated by error-prone recombination repair as it still occurs frequently in the absence of *recA* (Extended Data Fig. 7e). Third, we examined whether a commonly occurring G-T wobble mismatch, which is generated by the replicative DNA polymerase and efficiently corrected by mismatch repair[28], accounts for this mutation. Inactivating mismatch repair increased the mutation rate of *thyP3* by ~60 fold

similar to other mutation assays[18] and increased T→C substitutions at hotspots in the coding sequence by ~1000 fold (Extended Data Fig. 8f, g). Strikingly, we did not find any T_{-7}→C_{-7} substitution upon screening ~1000 mismatch repair mutants, suggesting that T_{-7}→C_{-7} is not generated via G-T mismatch.

After ruling out these known models of mutagenesis, we propose a new model that explains the frequent T_{-7}→C_{-7} substitutions based on the structure of the bacterial promoter open complex where the −10 element is single-stranded[25,29,30]. Specifically, during transcription initiation, T_{-7} on the non-template strand is buried in a sigma factor pocket, and its complementary base on the template strand (A_{-7}) is unpaired and vulnerable to spontaneous deamination to hypoxanthine[27] (Fig. 4d). Hypoxanthine can base pair with cytosine during replication, leading to the T_{-7}→C_{-7} mutation. This model is further supported by our data that treating cells with nitrous acid, an inducer of base deamination, leads to increased frequency of T_{-7}→C_{-7} mutation, which is more pronounced in the hypoxanthine-DNA glycosylase mutant (Fig. 4e), supporting hypoxanthine as the premutagenic intermediate. The cellular adenine deaminase is not a major factor responsible for T_{-7}→C_{-7} mutation (Extended Data Fig. 8h), indicating that the A_{-7} is spontaneously deaminated while sequestered within the transcription initiation complex. It is likely that other bases within the promoter open complex can also be mutated via deamination, although those mutations do not completely abolish gene expression thus cannot be identified by our assay. Our work thus uncovers a mechanism that implicates in general the greater susceptibility of promoters to mutations.

Our proposed mechanism represents a novel mutagenesis pathway that is distinct from TAM[10], which introduces substitutions within the transcribed sequence via deamination on the nontemplate strand, while the template strand of the coding sequence is protected by base pairing with nascent RNA (i.e. RNA-DNA hybrid). In contrast, the promoter is upstream of the transcription start site, thus is not protected by RNA-DNA hybrid and vulnerable to deamination or other premutagenic DNA damage upon open complex formation (Fig. 4d). We propose a model that head-on replication interferes with RNA polymerase escape from the promoter, rendering the promoter open complex more susceptible to premutagenic DNA damage, subsequently leading to mutations.

Our work reveals two types of collision-induced mutations, indels and promoter substitutions, which are generated by distinct mechanistic pathways likely resulting from mutual antagonism between replication and transcription upon collision. Our work supports the hypothesis that collision-induced mutagenesis contributes to the evolution of the strong co-directional bias of essential genes[5] and reveals orientation-biased promoter mutation underlying this conserved aspect of genome organization. We suspect that these mutation signatures have important implications not only in fitness and evolution of bacteria but also in higher organisms including humans. Indels can lead to copy number variation, a significant cause of genetic diseases. Mutations in *cis*-regulatory elements lead to misregulation of gene expression, and *cis*-regulatory elements are found to be more susceptible to mutagenesis than coding regions in eukaryotic genomes[17]. Thus, harmonizing replication with transcription is a key factor in fitness and genome evolution across domains of life.

Methods

Media and growth conditions

Unless otherwise indicated, cells were grown in S7 defined medium[31] containing 50 mM MOPS and supplemented with 1% glucose, 0.1% glutamate, 40 μg/ml tryptophan, and 20 μg/ml thymine (Sigma-Aldrich) at 37 °C with vigorous shaking, and plated on solid medium (Spizizen's medium), supplemented with 1% glucose, 0.1% glutamate, 40 μg/ml tryptophan, and 20 μg/ml thymine. Trimethoprim (RPI Research Products International Corp.,) was added to plates at a final concentration of 5 μg/ml for selecting loss-of-function mutations in *thyP3* gene. To induce expression of *thyP3*, isopropyl β-D-1-thiogalactopyranoside (IPTG) was added to the medium at a final concentration of 1 mM.

Strain construction

Strains used are derivatives of the wild-type strain *B. subtilis* 168 (JDW437) unless otherwise stated and are listed in Extended Data Table 1. The plasmids and PCR primers are listed in Extended Data Tables 1 and 2 respectively. The *thyP3* strains were created in the Δ*thyA* (JDW1543) background. *thyA* was deleted using the markerless deletion method[32] with plasmid pJW395. The head-on *thyP3* strain JDW1544 was generated by transforming JDW1543 with linearized plasmid pJW396. The co-directional *thyP3* strain JDW1563 was generated by transforming JDW1543 with linearized plasmid pJW397. Swapped head-on and co-directional *thyP3* strains JDW1900 and JDW1901 were created by transforming JDW1543 with linearized plasmid pJW430 and pJW431, respectively. The head-on *thyP3* strain (JDW1176) in Δ*thyA* Δ*thyB* background was created by transforming JDW942 with linearized plasmid pJW331. The *lacZ* reporter strains used in competition assays were created by transforming the respective *thyP3* wild-type or mutant strains with linearized plasmid pJW417.

Plasmid pJW395 was constructed to create a markerless deletion of *thyA*, by inserting *thyA* upstream homologous sequence (PCR amplified by primers oJW1052/oJW1053) and downstream homologous sequence (PCR amplified by primers oJW1054/oJW1055) between the *Eco*RI and *Bam*HI sites of pJW299. Plasmid pJW331 was constructed by inserting *thyP3* gene between SalI and SphI sites of pDR90. The *thyP3* gene sequence, including its promoter, was amplified from genomic DNA of JDW941 using oJW760/oJW761. Plasmid pJW396 was constructed by inserting the *thyP3* gene between *Sal*I and *Sph*I sites of pDR110. Plasmid pJW397 was constructed by excising out the P_{spank}-*thyP3* region from pJW396 by double restriction digest with *Eco*RI and *Sph*I and replacing it with P_{spank}-*thyP3* sequence in the inverse orientation between the *Eco*RI and *Sph*I sites. The P_{spank}-*thyP3* sequence for inversion was amplified from pJW396 using primers oJW785 and oJW1137.

Plasmid pJW430 was created by Gibson assembly[33] of a DNA fragment containing the *lacI*-P_{spank}-*thyP3-spec* sequences and the portion of the pDR110 plasmid backbone containing the plasmid replication origin, amp^R, and *amyE* front (5′) and back (3′) homology sequences. The DNA fragment with *lacI*-P_{spank}-*thyP3-spec* sequences was amplified from pJW397 using oJW1336/oJW1339. The pDR110 backbone fragment was amplified from pDR110 using oJW1337/oJW1338. Plasmid pJW431 was created in the same way as

plasmid pJW430, except the DNA fragment with *lacI-P*$_{spank}$*-thyP3-spec* sequences was amplified from pJW396, instead of pJW397, using the same primers. Plasmid pJW417 was created by Gibson assembly[33] of a DNA fragment containing the *spoVG-lacZ* sequences and a portion of pDR110 plasmid containing the *P*$_{pen}$ promoter and *lacA* locus 5′ and 3′ homology sequences for integration. The DNA fragment containing the *spoVG-lacZ* sequence and plasmid backbone were amplified from pEX44 using oJW1200/oJW1201 and oJW1213/oJW1214 respectively. The *P*$_{pen}$ promoter was amplified from pDR110 using oJW1202/oJW1203. The *lacA* 5′ and 3′ homology regions were amplified from the chromosomal DNA of *B. subtilis 168* using oJW1215/oJW1199 and oJW1204/oJW1216 respectively.

Deletion mutants of *yqjH* gene encoding PolIV (JDW2266), *adeC* encoding adenine deaminase (JDW2501), *recA* encoding the recombinase RecA (JDW2288) and *yxlJ* encoding hypoxanthine-DNA glycosylase (JDW2284) were obtained from the *Bacillus* genetic stock center (BGSC). Co-directional (JDW1563) and head-on *thyP3* (JDW1544) strains were transformed with the genomic DNA of each mutant and were selected on erythromycin plates at 37 °C. Deletion of each gene was confirmed by PCR (*yqjH*-oJW1900/1901; *adeC*-oJW1904/1905; *recA*-oJW2008/2009; *yxlJ*-oJW1906/1907) and *recA* mutant was also tested for UV sensitivity. Deletion of mismatch repair genes *mutS* and *mutL* was created by transforming the genomic DNA of JDW1297 into co-directional (JDW1563) and head-on *thyP3* (JDW1544) strains and were selected on kanamycin plates at 37 °C. The kanamycin gene insertion inactivated both mismatch repair genes and insertion was confirmed by PCR (oJW1902/1903).

Forward mutation fluctuation tests

Fluctuation tests were performed to measure the forward mutation rate. All the *thyP3* strains were in the background Δ*thyA thyB*$^{+}$. For each biological repeat, at least 30 parallel cultures of 0.1 ml in 96-well plates were set up for each strain at a dilution of 1×10^{-5} and grown at 37 °C to OD_{600} = 0.4–0.6 in S7 minimal medium with 20 μg/ml thymine and with 1 mM IPTG (induced transcription) or without IPTG (un-induced transcription). Loss-of-function mutations in *thyP3* genes confer resistance to trimethoprim (TMP). For selection of mutants, 0.1 ml of culture was plated on Spizizen's minimal medium containing 20 μg/ml thymine, 1 mM IPTG and 5 μg/ml trimethoprim. Plates were incubated at 45 °C, and the number of trimethoprim resistant colonies were counted at 48 h (day 2) and 72 h (day 3) of incubation. Serial dilutions of at least 3 cultures were plated on non-selective medium to determine the average colony forming units (CFU). The number of mutations per culture (*m*) was estimated using the MSS-Maximum Likelihood Estimator (MSS-MLE) method through the Fluctuation AnaLysis CalculatOR (FALCOR) web tool[34], and the mutation rate per cell per generation was calculated by $m/(2*N_t)$, where N_t is the average number of cells across cultures in a fluctuation test[21]. Fluctuation tests of the deletion mutants were performed as described for the wild-type strains above except for *recA* and *mutSL* deletion strains. Since *recA* mutant showed increased sensitivity to trimethoprim, selection of *thyP3* mutants was done at 1 μg/ml concentration of trimethoprim and mutant colonies were obtained from day 4 and day 5 after incubation. Fluctuation tests with *mutSL* mutants were performed identical to wild-type, except that the cultures were diluted 1:20 for selection on trimethoprim plates,

since inactivation of mismatch repair increases the mutation rate. The mean of mutation rates from n≥3 independent experiments was plotted with error bars representing standard error. Statistical significance was calculated by paired Student's *t*-test of ln(m) values[21]. We employed a mutation assay for nalidixic acid resistance, which is conferred by mutations in *gyrA* gene encoding DNA gyrase, to examine whether mutation rate is different outside *thyP3* locus between the co-directional and head-on *thyP3* strains. For measurement of the mutation rate for nalidixic acid resistance (Nal^R), at least 30 parallel 1 ml were grown in test tubes to OD_{600} = 0.4–0.6 and entire cultures were plated on minimal medium containing 20 μg/ml thymine, 1 mM IPTG, and 50 μg/ml nalidixic acid (Sigma-Aldrich). Plates were incubated at 45 °C for 48 h, and the number of plates with no Nal^R colonies was counted. Serial dilutions were plated on non-selective medium to count the number of CFU. The number of Nal^R mutations per culture (*m*) was estimated using the P_0 method and the mutation rate was calculated by $m/(2*N_t)$[21]. Error bars represent the standard error from at least 3 independent experiments.

Mutation spectra and rates of different mutations

To obtain the mutation spectrum, genomic DNA from one colony per selective plate was extracted by using the *prep*GEM Bacteria kit (Zygem Corp., New Zealand) and *thyP3* was PCR amplified and sequenced using primers oJW1013 and oJW1335. The rate of individual mutation was determined by multiplying the total mutation rate by the proportion of different mutations in the mutation spectra as described[35]. Statistical significance of differences between co-directional and head-on strains for different mutation types was obtained using Student's *t*-test.

Real Time Quantitative Reverse Transcription PCR (qRT-PCR)

Measurement of *thyP3* transcription levels was performed by qRT-PCR. Cultures were grown in minimal media with 20 μg/ml thymine, with or without 1 mM IPTG, to OD_{600} 0.4 – 0.6. RNA was isolated using the Qiagen RNeasy kit and reverse-transcribed using SuperScript III reverse transcriptase (Life Technologies). Real-time PCR was performed using SYBR green master mix (Applied Biosystems) with primers oJW1217/oJW1218 for amplifying the beginning of *thyP3*. The *accA* gene transcript amplified with primers oJW1221/oJW1222 was used as an internal control[36].

Competition assay

Competition experiments were performed between strains carrying the wild-type and mutant *thyP3*. Strains were grown in S7 minimal medium supplemented with 1% glucose, 0.1% glutamate, 40 μg/ml tryptophan and 1 mM IPTG. Strains in competition were distinguished by integrating a *lacZ* reporter gene at the *lacA* locus in the chromosome, enabling the competitors to be distinguished on X-gal indicator plates in which $LacZ^-$ and $LacZ^+$ form white and blue colonies respectively. The *lacZ* marker was swapped between the competing strains to negate any growth effect from the *lacZ* marker. Strains were preconditioned in the growth medium to saturation. Cultures were then mixed in 1:1 ratio, and serial passage was performed with 1:1000 dilutions (~10 generations per cycle) every 12 h until 70 generations. The ratio of mutant over wild-type at each cycle was estimated by plating the serially diluted cultures on SPII minimal plates supplemented with 40 μg/ml tryptophan, 20 μg/ml thymine

and 40 μg/ml X-gal (5-bromo-4-chloro-3-indolyl-β-d-galactopyranoside) at 37 °C. Growth rate was calculated using the initial and final cell densities for each strain in the pair, and the relative fitness was calculated as the ratio of growth rates of mutant over wild-type cells[7]. Assays were performed with three independent replicates of the mutant tagged with *lacZ* and another three in which the wild-type was tagged with *lacZ*. Relative fitness was then expressed as the mean±SD of replicates with and without the marker. In order to rule out reversion of the mutant *thyP3* strain during competition growth, strains were plated at the end of 70 generations on X-gal indicator plates with and without thymine at 45 °C and also on trimethoprim plates; only the wild-type formed colonies on plates without thymine and the mutants formed colonies only on plates with thymine. As expected, wild-type did not form colonies on trimethoprim, while the mutants formed colonies. These indicate that the mutants did not revert during competitive growth nor did the wild-type acquired a *thyP3* mutation.

Restriction digest screen of promoter mutation

To screen for $T_{-7}\rightarrow C_{-7}$ mutation in the promoter, the first half of the *thyP3* fragment including the promoter region was PCR amplified with primers oJW1335 and oJW1011 from mutant DNA. The PCR fragment was digested with AflIII enzyme (NEB) and digested products were analyzed in 1.5% agarose gel. PCR fragments containing the $T_{-7}\rightarrow C_{-7}$ mutation are digested by AflIII, whereas wild-type fragments are not digested (Extended Data Fig. 8e).

Sequence logo of the −10 element of SigA dependent promoters

We obtained the sequences of the −10 element of all experimentally validated SigA-dependent promoters (n=358) available at the DBTBS database[37] and used the WebLogo tool[38] to generate the consensus motif with the default parameters to show the genome-wide conservation of the −10 element.

Comparative genomic and molecular evolutionary analyses

For comparative genomic and evolutionary analyses, we used the completed genomes of 8 strains of *B. subtilis* and one *B. amyloliquefaciens* strain, a close relative of *B. subtilis*. The analyzed genomes are listed in Extended Data Table 2. Complete genomes, amino acid and nucleotide sequences of genes and intergenic sequences, and gene annotation information were downloaded from the Integrated Microbial Genomes (IMG) database[39]. Core genes from *B. subtilis* and *B. amyloliquefaciens* were identified by standard all-against-all reciprocal best-hit method using BLASTP. Best bi-directional hits were considered when the alignment had >85% identity with 85% coverage length at an E-value cut-off of 10^{-20}. We eliminated any gene annotated as pseudogene and containing ambiguous nucleotides from the analysis.

To assign genes to leading and lagging strand, we obtained the sequence coordinates of *oriC* and *dif* sites from the DoriC database[40] for each genome, and using these coordinates in combination with transcript orientation information from the genome annotation files (plus or minus strand), genes were assigned to leading and lagging strands. All genes analyzed were present on the same strand (either leading or lagging) in all the genomes analyzed.

To extract promoter sequences, experimentally validated promoter annotations were obtained for the core genes of *B. subtilis* strain 168 from the DBTBS database[37]. Sequence encompassing the transcription start site (+1), the −10 and −35 elements of the promoter was obtained. Using these promoter sequences as references, homologous promoters from the other genomes of *B. subtilis* and *B. amyloliquefaciens* were obtained using the blastn-short algorithm of BLASTN employing the 75% identity over 80% alignment coverage with e-value less than 10^{-5}. We obtained 179 promoters (147 and 32 for leading and lagging strand genes, respectively).

The amino acid sequences and the corresponding nucleotide sequences of protein-coding core genes were aligned using the G-INS-i algorithm of the MAFFT alignment program (v7.012b)[41]. Further, to produce high quality alignments, we used the PAL2NAL program (v12.1)[42], which produces codon-based alignments from aligned protein sequences and the corresponding DNA sequences. Additionally, PAL2NAL reports whether the protein and nucleotide sequences have mismatches or in-frame stop codons. The codon-based alignments of the core genes generated by PAL2NAL did not contain any mismatches or in-frame stop codons, which ensured the high quality of the alignments.

For aligning the promoters, we used the E-INS-i algorithm of the MAFFT alignment program, which is optimized for aligning highly conserved motifs interspaced between weakly conserved regions. The alignments of the experimentally validated promoters were manually inspected for any misalignments.

Estimation of nucleotide substitutions in promoters

To estimate nucleotide substitutions in promoters, we first constructed phylogeny using the concatenated sequence of the core genome genes, i.e., genes present in all the analyzed genomes. The aligned nucleotide sequences were concatenated to create a single sequence for each analyzed strain. Phylogeny was constructed using PhyML program[43] with 500 bootstrap replicates. The substitution model used was General Time Reversible model (GTR) with discrete gamma model, and gamma parameter was estimated.

For each promoter, substitutions were estimated by pairwise comparison of the different strains using the baseml program of PAML package[44]. Baseml program uses a maximum likelihood approach to estimate nucleotide substitutions, based on an input phylogenetic tree. We used the maximum likelihood phylogenetic tree generated earlier and the substitution model was GTR. The rest of the parameters were default. Then for each promoter, mean substitutions per site were calculated and the distribution of mean pairwise substitution rates was compared between leading and lagging strand promoters. Mann-Whitney U test was used to determine statistical significance.

For comparing the mutation rates between promoters with and without transcription factor binding, we used the population genetic parameter Watterson's estimator of Theta (θ_W). Since theta (θ_W) is a population genetic parameter, it is well suited for analyzing within species sequence polymorphism and thus θ_W serves as a proxy for mutation rate of a given promoter. We calculated θ_W for the total number of mutations in the high quality sequence alignment for each promoter across the 8 strains of *Bacillus subtilis* (Extended Data Table 2)

using the DnaSP software (v5)[45]. Promoters with experimentally validated transcription factor binding were obtained from the DBTBS database[37]. Sequence covering the +1 site, −10 and −35 elements that includes the transcription factor-binding site were used for constructing the alignment as described above. A total of 33 different transcription factors that are experimentally validated in *B. subtilis* were used (Extended Data Table 2). Mann-Whitney U test was used to determine statistical significance.

Nitrous acid mutagenesis

Nitrous acid is known to strongly deaminate purines and pyrimidines in DNA. Adenine is deaminated to hypoxanthine[46] that produces A:T to G:C transition. We subjected the wild-type and *yxlJ* (encoding hypoxanthine-DNA glycosylase)[47] mutant strains carrying the head-on *thyP3* reporter under induced transcription to nitrous acid treatment following the protocol reported before[48]. Briefly, cells were grown in 5 mL of S7 minimal medium with 20 μg/ml thymine, 40 μg/ml tryptophan and with 1 mM IPTG for 12 hours to saturation. To the saturated cultures 1 mL of 8.7 M $NaNO_2$ (nitrous acid dissolved in sodium acetate buffer pH 4.6) (Sigma-Aldrich) was added and incubated at room temperature for 60 minutes. As a control, cells were treated with the sodium acetate buffer in parallel. Cells were then spun down, washed and re-suspended in the growth medium and 1 mL of culture was used for determining the CFU and the rest of the culture were plated on minimal plates supplemented with 20 μg/ml thymine, 40 μg/ml tryptophan, 1 mM IPTG and 5 μg/ml trimethoprim for selecting trimethoprim resistance mutants. The same was performed for buffer treated cells except that 0.1 mL of culture was used to determine CFU and 0.1 mL was plated for selecting trimethoprim resistant colonies. After 2 days of incubation, trimethoprim resistance colonies appeared, and as described before the *thyP3* gene was PCR amplified and screened for $T_{-7}\rightarrow C_{-7}$ mutation. Mutation frequency was calculated by dividing the number of trimethoprim resistant colonies by number of colonies on nonselective plate. Experiment was done in triplicate and error bars represent s.e.m. Statistical significance was obtained using Student's *t*-test.

Extended Data

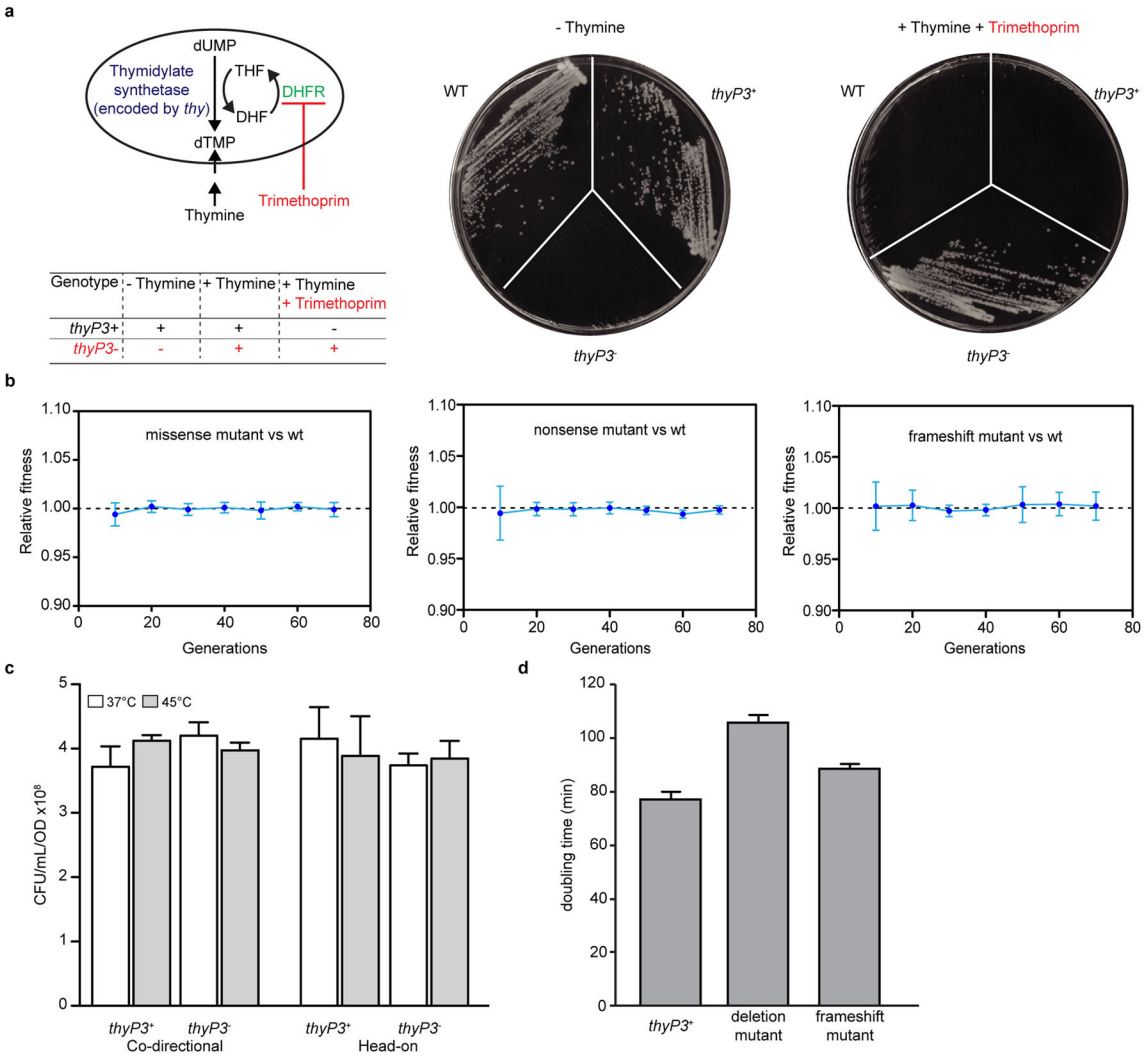

Extended Data Figure 1. Development of a forward mutation assay that detects loss-of-function mutations in B. subtilis

a, Simplified diagram of thymidine monophosphate (dTMP) synthesis. The phage-encoded *thyP3* encodes thymidylate synthetase, which synthesizes dTMP and dihydrofolate (DHF) from dUMP and tetrahydrofolate (THF). DHF is recycled back to THF by dihydrofolate reductase (DHFR). Trimethoprim inhibits DHFR, thus blocking recycling of the essential cofactor THF and available THF is depleted by active thymidylate synthetase and cell growth is inhibited. Because cells with active thymidylate synthetase rely solely on endogenous dTMP synthesis, *thyP3*$^{+}$ cells are sensitive to trimethoprim and loss-of-function mutations in *thyP3* lead to trimethoprim resistance, which is the basis for the forward mutation assay. Viabilities of wild-type (*thyA*$^{+}$ *thyB*^{ts}), *thyP3*$^{+}$ (Δ*thyA thyB*^{ts} *thyP3*$^{+}$) and *thyP3*$^{-}$ (Δ*thyA thyB*^{ts} *thyP3*$^{-}$) cells are shown in the table and representative colonies (at 45 °C) are shown on the right. **b,** Competition between strains carrying wild-type (wt) and mutant *thyP3* in Δ*thyA thyB*^{ts} background to determine if there is any selective pressure on

different mutants during growth phase at permissive temperature (37 °C). Relative fitness (mean±s.d) of six replicates is shown. **c,** Shifting the temperature to 45 °C does not affect plating efficiency during selection for trimethoprim resistance. Wild type and mutant *thyP3* cells were grown at 37 °C and plated on solid medium supplemented with IPTG+thymine at 37 °C and 45 °C, and CFU/mL/OD was determined. Mean±s.d of 3 replicates is shown. **d,** *thyP3* mutants have growth defects without *thyB*^{ts}. The doubling times of *thyP3* mutant (a deletion and a frame-shift mutant) in the Δ*thyA* Δ*thyB* background at 37 °C are longer, indicative of growth defects in the absence of the backup gene *thyB*. Mean±s.d of 3 replicates is shown. For b and d, the mutant strains are listed in Extended Data Table 1.

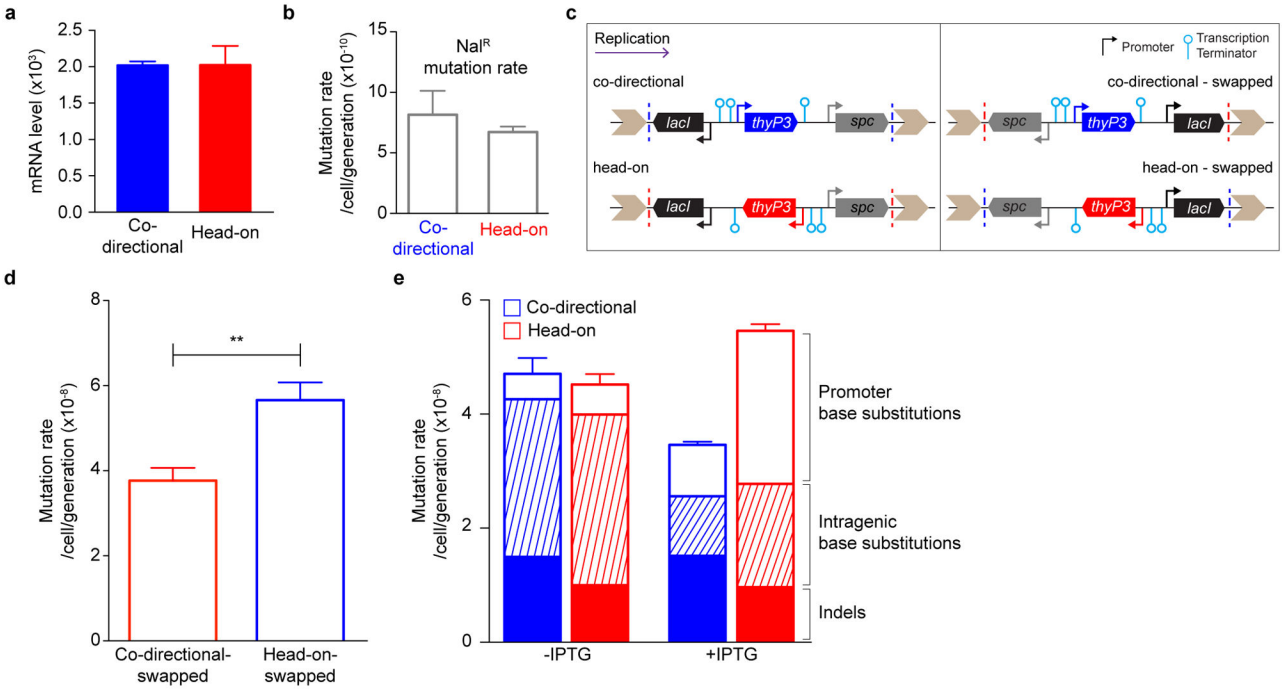

Extended Data Figure 2. Expression level and mutation rate of *thyP3*

a, *thyP3* expression in co-directional and head-on orientations. Using real-time quantitative PCR, mRNA level of *thyP3* in the co-directional and head-on strains under induced (+IPTG) condition was measured and normalized to the reference gene *accA*. Since level of expression is similar between the strains, the observed difference in *thyP3* mutation rate between co-directional and head-on orientations (Fig. 1d) is not caused by intrinsic differences in the expression level of *thyP3*. **b,** The orientation-specific difference in *thyP3* mutation rate is not due to global increase of mutagenesis in the head-on strain. As a control to show that the increase in mutation rate is local to *thyP3* reporter, we measured the mutation rate for resistance to nalidixic acid (Nal^{R}, conferred by mutations in *gyrA* gene) in co-directional and head-on strains. Since the Nal^{R} mutation rates in the two strains were similar, we conclude that the observed increase in head-on mutation rate is specific to *thyP3* gene. **c,** Schematics of the co-directional and head-on *thyP3* constructs (left) and an additional control to examine the effect of the genomic context on *thyP3* mutagenesis, the neighboring genes were swapped (right). In each construct, the *thyP3* gene is flanked by the *lacI* gene and the spectinomycin-resistance gene. The reporter constructs were integrated

into the chromosome at the *amyE* locus by double crossover. The direction of replication is shown at the top. The co-directional-swapped strain was created by inverting the *lacI-thyP3-spc* from the head-on strain and the head-on-swapped construct was created by inverting the same from co-directional strain. Thus the swapped constructs switch the neighboring transcription units. The dotted lines in each construct show the swapping boundary. **d,** The mutation rate of swapped head-on strain is still higher than swapped co-directional strain when transcription is induced (+IPTG), indicating that the difference in mutation rate between reporter strains is not due to the direction of *thyP3* relative to its neighboring genes. **e,** Mutation rate of co-directional and head-on *thyP3* under uninduced (−IPTG) and induced (+IPTG) transcription. The rate of each class of mutations obtained under each condition is also depicted within each bar. For b, d and e mean±s.e.m of n≥3 independent experiments is shown. (**P<0.01, Student's *t*-test).

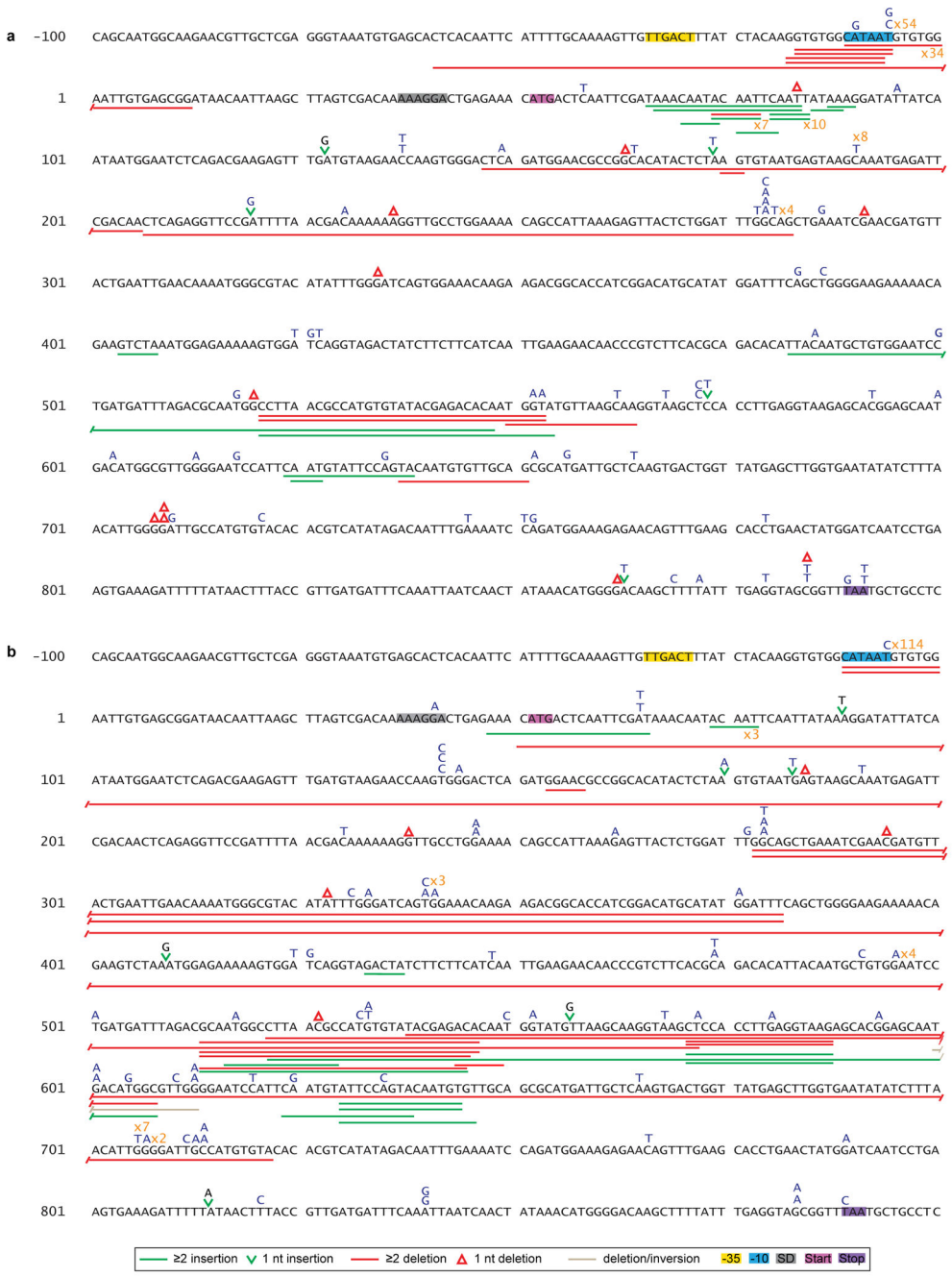

Extended Data Figure 3. Mutation spectra of *thyP3* under induced transcription

Illustrations of the mutation spectra of the *thyP3* mutants obtained from fluctuation tests of: **a,** co-directional (n=214) and **b,** head-on (n=232) strains when transcription is induced (+IPTG). The *thyP3* coding sequence with its promoter is shown. Sequence coordinates are indicated with reference to +1 transcription start site. The symbols used to represent different mutations are shown at the bottom, and base substitutions are shown in blue color above the sequence. The numbers marked in orange next to a mutation denote the frequency.

The promoter elements, Shine-Dalgarno (SD) sequence, and start and stop codons are highlighted in each spectrum.

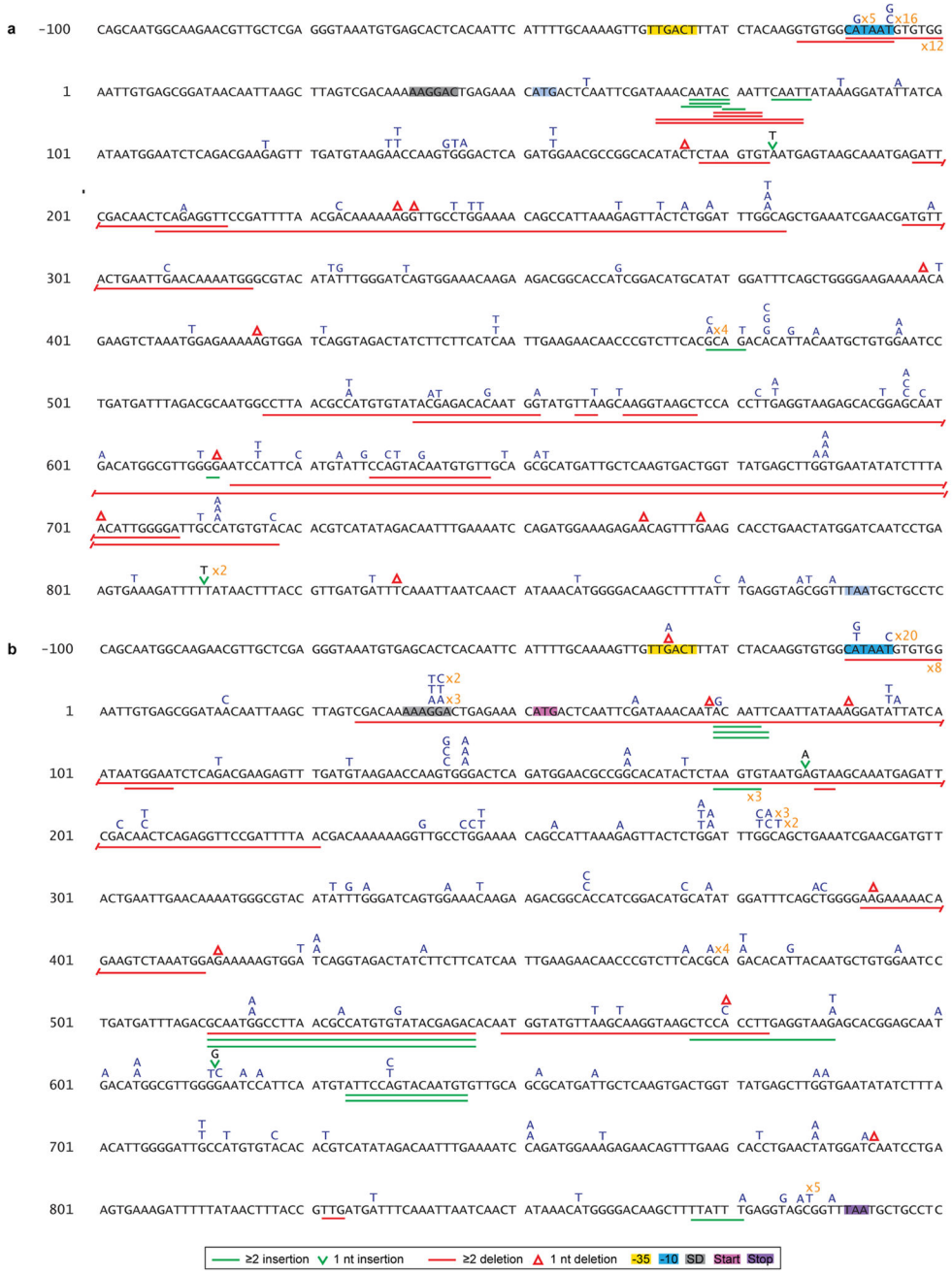

Extended Data Figure 4. Mutation spectra of *thyP3* under un-induced transcription

Illustrations of the mutation spectra of the *thyP3* mutants obtained from fluctuation tests of: **a,** co-directional (n=163) and **b,** head-on (n=178) strains when transcription is not induced (−IPTG). The *thyP3* coding sequence with its promoter is shown. Sequence coordinates are indicated with reference to +1 transcription start site. The symbols used to represent different mutations are shown at the bottom, and base substitutions are shown in blue color

above the sequence. The numbers marked in orange next to a mutation denote the frequency. The promoter elements, Shine-Dalgarno (SD) sequence, and start and stop codons are highlighted in each spectrum.

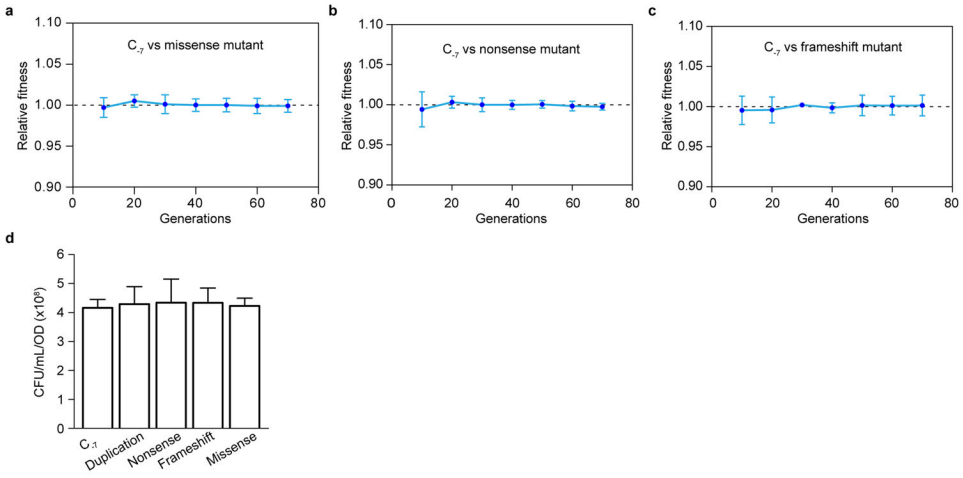

Extended Data Figure 5. Absence of selection bias in *thyP3* forward mutation assay

Growth competition experiments were performed between the C_{-7} promoter mutant against the following mutants: **a,** missense mutant, **b,** nonsense mutant and **c,** frameshift mutant. Each mutant was competed against the C_{-7} promoter mutant to check if there is a competitive disadvantage for a mutant that has a mutation within the coding sequence, which may explain the high frequency of C_{-7} mutation compared to other mutations. The results show no fitness disadvantage for any of the mutants tested suggesting that the high frequency of C_{-7} promoter mutation is not due to a selection bias. For a–c mean±s.d of six replicates is shown and mutants competed are indicated within the plot. **d,** Plating efficiency of different *thyP3* mutants. Plating efficiency was determined to check whether different classes of *thyP3* mutants have differences in their plating efficiency on trimethoprim selection plates at 45 °C, which may explain the variation in the mutation rates and spectrum. The result shows similar plating efficiency among the different mutants, suggesting that plating efficiency does not underlie the variation in the observed mutation rates. The different mutants tested are indicated on the X-axis. Mean±s.d of 3 replicates is shown. The mutant strains are listed in the Extended Data Table 1.

b

Mutation rate of indels normalized to the length of the region (x10^{-11})

Position	Co-directional -IPTG	Head-on -IPTG	Co-directional +IPTG	Head-on +IPTG
5'	0.96	0.61	1.12	0.48
3'	0.52	0.55	0.38	1.18
Promoter	10.2	5.79	15.8	1.17

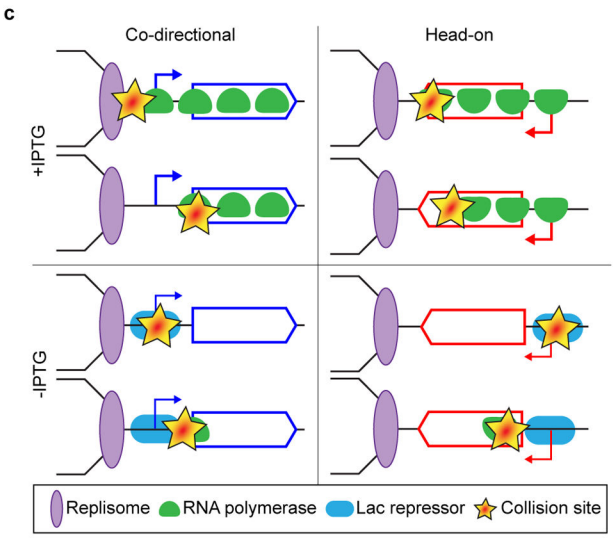

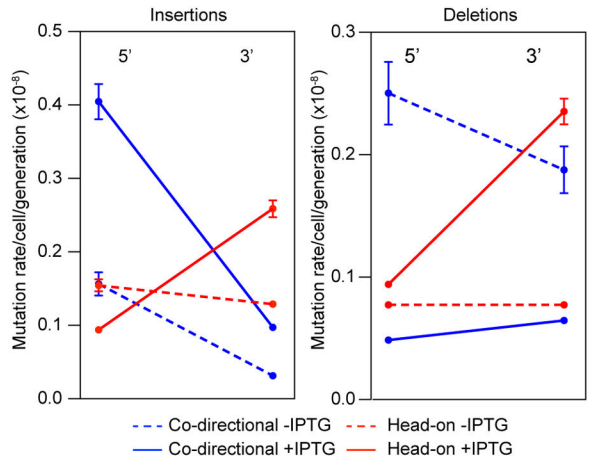

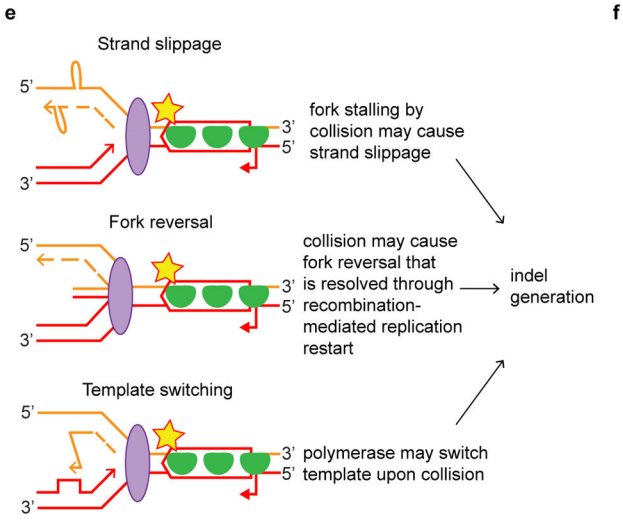

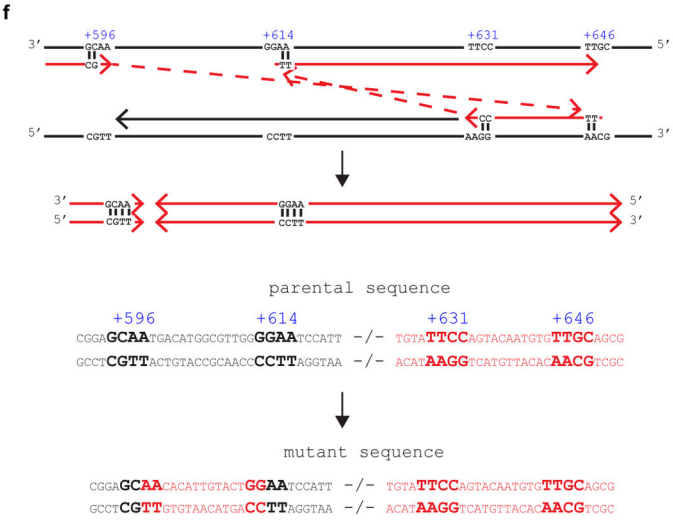

Extended Data Figure 6. Mechanism of indel generation

a, Representative deletion and duplication events in *thyP3*. A high frequency deletion and duplication event observed in *thyP3* gene in co-directional and head-on strains. The sequence coordinates are denoted and repeat sequence is underlined. **b,** Table showing the mutation rate of indels (≥3 bp) in intragenic region and promoter normalized by the length of the region suggests that the localized rate of indels is higher in the promoter than the intragenic region. **c,** First encounter between replication and transcription machineries generates indels. Model describing the first-encounter hypothesis proposed based on results presented in Fig. 2a–f. In co-directional orientation under induced transcription (+IPTG), when an array of RNA polymerase (RNAP) transcribe the gene the replisome is likely to

collide with the first transcription complex at the promoter or promoter-proximal regions. On the contrary, when transcription is induced in head-on orientation, the replisome encounters the first transcription complex from the 3′ end. In support of this first encounter model, when transcription is not induced (basal level) the density of RNAP is sparse along the gene, hence the site of collisions are altered. In addition, it is possible that under basal transcription, collision can occur between replisome and RNAP complex arrested at the promoter or with the Lac repressor, which may explain the relatively high frequency of deletion at the promoter. Thus the “first-encounter” model of replication-transcription collisions supports that collisions stall replisome progression triggering indel mutations. **d,** Mutation rate of insertions and deletions (≥3 bp) within the intragenic region plotted individually. Frequency of insertions is increased by transcription in both co-directional and head-on orientations, whereas deletion frequency is specifically increased in head-on orientation. Mean±s.e.m of n≥3 experiments is shown. **e,** Models illustrating the different pathways that can lead to generation of indels following head-on collision-induced replication stalling: slippage, fork-reversal or template switching. **f,** Illustration of a complex mutation observed in *thyP3* that is likely generated via Microhomology-Mediated Break Induced Replication (MMBIR). The complex mutation encompassing a deletion and insertion of an inverted region was observed under induced transcription in head-on orientation. The sequence coordinates are marked on the top with reference to the transcription start site (+1).

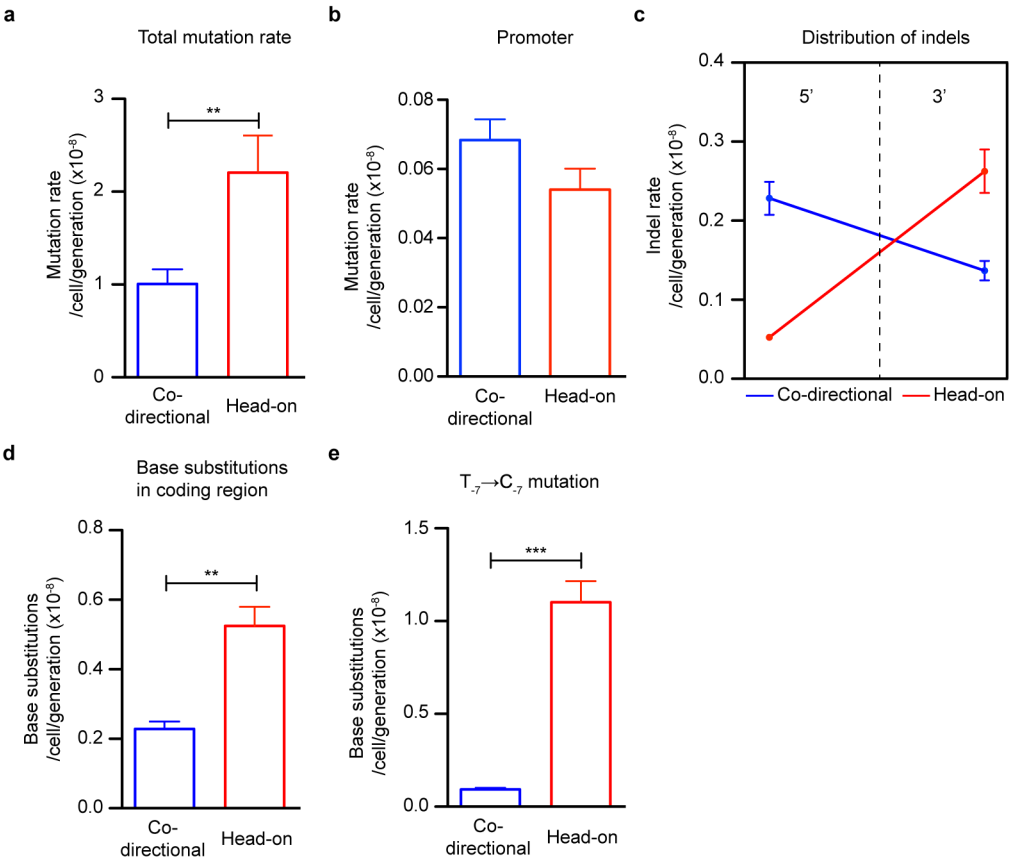

Extended Data Figure 7. Role of recombination protein RecA in collision-induced mutations

a, Mutation rates of co-directional and head-on *thyP3* strains for trimethoprim resistance in Δ*recA* background. Similar to wild-type the mutation rate of head-on is higher than the co-directional strain, although the total rate of mutation is decreased in Δ*recA* background. **b,** Rate of ≥3 bp indels at the promoter in co-directional orientation is strongly decreased in Δ*recA* cells suggesting that indels at the promoter are mostly RecA-dependent. **c,** Intragenic distribution of ≥3 bp indels in Δ*recA* is similar to the distribution observed for wild-type (Fig. 2f), thus suggesting that RecA is not necessary for the collision-induced indels within coding region. **d,** Mutation rate of base substitutions in Δ*recA* cells is higher in head-on than co-directional orientation. **e,** The rate of $T_{-7} \rightarrow C_{-7}$ mutation is higher in head-on relative to co-directional orientation in Δ*recA* cells, thus promoter substitutions can occur at a higher rate independent of recombination-mediated repair. All the fluctuation tests in Δ*recA* background were performed under inducing conditions (+IPTG). For a–e mean±s.e.m of n≥3 experiments is shown. (**P<0.01; ***P<0.001; Student's *t*-test)

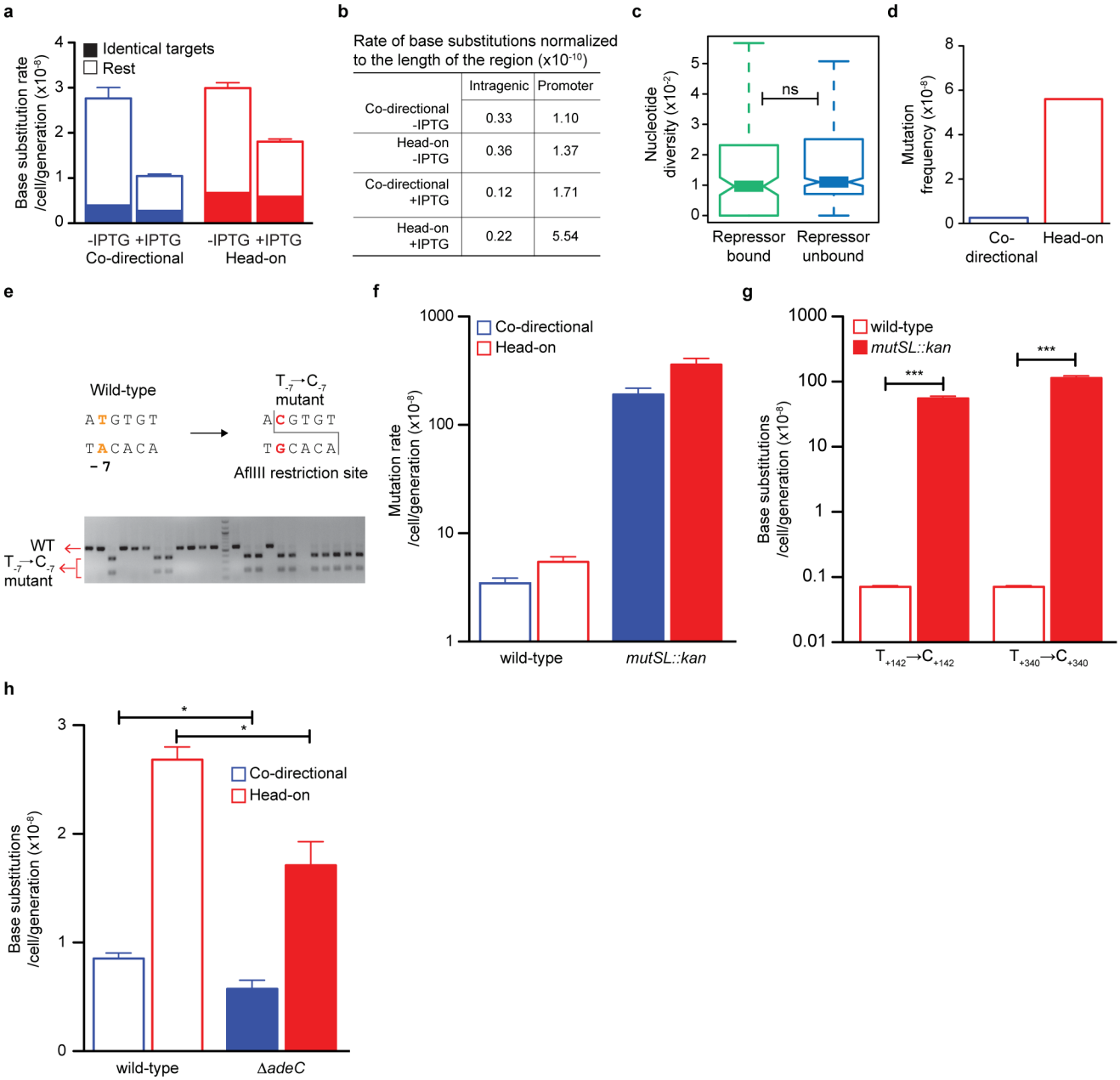

Extended Data Figure 8. Base substitutions and the role of mismatch repair and enzymatic adenine deamination

a, IPTG-induction does not affect the base substitution rate in coding region of *thyP3* when considering identical target sites, indicating that collisions may not be a major source of these mutations. In yeast, it was shown that transcription-associated mutagenesis is proportional to level of transcription[10]. In *B. subtilis*, the total rate of base substitutions in the coding region significantly decreases upon IPTG induction, which could be due to an unidentified transcription dependent mutation-correction mechanism, or due to increase of target size of base substitutions in the coding sequence in un-induced (basal) transcription. **b,** Table showing the rates of base substitutions in coding region and promoter of *thyP3*

normalized by length of the region. Localized substitution rates are higher in the promoter than coding sequence, thus suggesting that collision has more drastic effect on promoter substitutions. **c,** Comparative genomic analysis of mutation rates of promoters with and without repressor binding. Nucleotide diversity per site (Theta) was calculated for each promoter across different strains of *Bacillus subtilis*. The comparison shows no significant difference in nucleotide diversity between repressor-bound promoters and rest of the promoters, indicating that repressor binding may not affect the substitution rate of a promoter. Whole genomes and the repressors analyzed are listed in Extended Data Table 2. (ns-not significant P>0.05; Mann-Whitney U test). **d,** The mutation frequency of $T_{-7}\rightarrow C_{-7}$ mutation is higher in head-on than co-directional orientation in *E. coli*. The mutation frequency was calculated here from the plasmid-based forward mutation assay data reported by Yoshiyama et al., (2001)[26]. **e,** The restriction digestion-based assay to screen for $T_{-7}\rightarrow C_{-7}$ mutation. Wild-type promoter sequence does not have an AflIII restriction site, whereas the promoter $T_{-7}\rightarrow C_{-7}$ mutation will be digested by AflIII, which is illustrated by a representative agarose gel. **f,** Mismatch repair mutant (*mutSL::kan*) shows an expected increase (~60-fold) in total mutation rate of *thyP3* in both co-directional and head-on orientation compared to wild-type. The mutation rates of the wild-type strains are presented before in Fig. 1d. **g,** Mismatch repair mutant shows a drastic ~1000 fold increase in mutation rate of T→C substitution hotspots within the coding sequence of head-on *thyP3*, indicating that mismatch repair corrects T→C substitution within coding sequence. **h,** Deletion of *adeC* gene encoding adenine deaminase modestly reduces the mutation rate of $T_{-7}\rightarrow C_{-7}$ substitution in both co-directional and head-on orientation compared to wild-type. For f–h mean±s.e.m of n≥3 experiments is shown. (*P<0.05; ***P<0.001; Student's *t*-test).

Extended Data Table 1

Strains and plasmids used in this study. a,Bacterial strains used in this study. **b,** Plasmids used in this study. BGSC - Bacillus Genetic Stock Center (http://www.bgsc.org)

a

Name	Genotype	Source
JDW437	(wild-type 168) *trpC2*	Lab stock
JDW941	151 *phi3T*	Ronald Yasbin
JDW942	168 *thyA*$^{-}$ *thyB*$^{-}$	Ronald Yasbin
JDW1297	PY79 *mutSL::kan*	Lyle Simmons
JDW1543	168 Δ*thyA*	This work
JDW1544	168 Δ*thyA amyE::*P_{spank}*-thyP3* (head-on) *spc*	This work
JDW1563	168 Δ*thyA amyE::*P_{spank}*-thyP3* (co-directional) *spc*	This work
JDW1711	168 Δ*thyA amyE::*P_{spank}*-thyP3* (head-on) *spc, lacA::*P_{pen}*-spoVG-lacZ*	This work
JDW1814	168 Δ*thyA amyE::*P_{spank}*-thyP3* (head-on) *spc, mutSL::kan*	This work
JDW1900	168 Δ*thyA amyE::spc-*P_{spank}*-thyP3* (head-on) *lacI*	This work
JDW1901	168 Δ*thyA amyE::spc-*P_{spank}*-thyP3* (co-directional) *lacI*	This work
JDW2054	168 Δ*thyA amyE::*P_{spank}*-thyP3* (head-on) $G_{+473}\rightarrow A_{+473}$ *spc*	This work
JDW2057	168 Δ*thyA amyE::*P_{spank}*-thyP3* (head-on) $T_{-7}\rightarrow C_{-7}$ *spc*	This work
JDW2185	168 Δ*thyA amyE::*P_{spank}*-thyP3* (head-on) $T_{+331}\rightarrow C_{+331}$ *spc*	This work

a

Name	Genotype	Source
JDW2190	168 Δ*thyA amyE::*P_{spank}*-thyP3* (head-on) $G_{+473}\rightarrow A_{+473}$ *spc, lacA::*P_{pen}*-spoVG-lacZ*	This work
JDW2192	168 Δ*thyA amyE::*P_{spank}*-thyP3* (head-on) $T_{-7}\rightarrow C_{-7}$ *spc, lacA::*P_{pen}*-spoVG-lacZ*	This work
JDW2266	168 Δ*yqjH*	BGSC
JDW2284	168 Δ*yxlJ*	BGSC
JDW2288	168 Δ*recA*	BGSC
JDW2491	168 *thyA*$^{-}$ *thyB*$^{-}$ *amyE::*$P_{spac(hy)}$*-thyP3* $\Delta_{+102\text{-}145}$ deletion *spc*	This work
JDW2492	168 *thyA*$^{-}$ *thyB*$^{-}$ *amyE::*$P_{spac(hy)}$*-thyP3* TT$_{+124}$ insertion *spc*	This work
JDW2501	168 Δ*adeC*	BGSC
JDW2529	168 Δ*thyA amyE::*P_{spank}*-thyP3* (head-on) *spc,* Δ*yqjH*	This work
JDW2530	168 Δ*thyA amyE::*P_{spank}*-thyP3* (co-directional) *spc,* Δ*yqjH*	This work
JDW2547	168 Δ*thyA amyE::*P_{spank}*-thyP3* (head-on) *spc,* Δ*adeC*	This work
JDW2548	168 Δ*thyA amyE::*P_{spank}*-thyP3* (co-directional) *spc,* Δ*adeC*	This work
JDW2598	168 Δ*thyA amyE::*P_{spank}*-thyP3* (head-on) *spc* Δ*recA,*	This work
JDW2612	168 Δ*thyA amyE::*P_{spank}*-thyP3* (co-directional) *spc,* Δ*recA*	This work
JDW2697	168 Δ*thyA amyE::*P_{spank}*-thyP3* (head-on) *spc,* Δ*yxlJ*	This work
JDW2746	168 Δ*thyA amyE::*P_{spank}*-thyP3* (head-on) $G_{+332}\rightarrow A_{+332}$ *spc*	This work
JDW2747	168 Δ*thyA amyE::*P_{spank}*-thyP3* (head-on) $G_{+332}\rightarrow A_{+332}$ *spc, lacA::*P_{pen}*-spoVG-lacZ*	This work
JDW2748	168 Δ*thyA amyE::*P_{spank}*-thyP3* (head-on) +1G_{+335} *spc*	This work
JDW2749	168 Δ*thyA amyE::*P_{spank}*-thyP3* (head-on) +1G_{+335} *spc, lacA::*P_{pen}*-spoVG-lacZ*	This work

b

Name	Genotype	Source
pDR90	*amyE::*$P_{spac(hy)}$ *amp spc*	David Rudner
pDR110	*amyE::*P_{spank} *amp spc*	David Rudner
pJW299	pEX44/I-*Sce*I site *amp cat*	Lab stock
pJW331	pDR90/*amyE::*$P_{spac(hy)}$*-thyP3*(head-on) *amp spc*	This work
pJW395	pJW299/Δ*thyA* I-*Sce*I site *amp cat*	This work
pJW396	pDR110/*amyE::*P_{spank}*-thyP3* (head-on) *amp spc*	This work
pJW397	pDR110/*amyE::*P_{spank}*-thyP3* (co-directional) *amp spc*	This work
pJW417	pEX44/*lacA::*P_{pen}*-spoVG-lacZ amp cat*	This work
pJW430	pDR110/*amyE::spc-*P_{spank}*-thyP3* (head-on) *lacI amp*	This work
pJW431	pDR110/*amyE::spc-*P_{spank}*-thyP3* (co-directional) *lacI amp*	This work

Extended Data Table 2

Primers, whole genome sequences and transcriptional regulators used in this study. a,Primers used in this study. **b,** Whole genome sequences used in this study. **c,** Transcriptional regulators analyzed in this study

a

Name	Sequence 5′ →3′
oJW760	GGTGTCGACATGACTCAATTCGATAAACAA

a

Name	Sequence 5′ →3′
oJW761	AATGGCATGCCAATATTTCACCAATTTCAT
oJW785	GTATGAATTCCAATATTTCACCAATTTCAT
oJW1011	GCGGATAACAATTTCACACAGGGTCTTCTTGTTTCCACTGAT
oJW1013	GCGGATAACAATTTCACACAGG CAATATTTCACCAATTTCAT
oJW1052	GGTAGAATTCACGTTATGGTTAAGATTCAA
oJW1053	AATGCTCGAGTATCCTTCTTTCATTTTCAG
oJW1054	GGTACTCGAGTAGCAGGTATCCTAATTTCA
oJW1055	AATGGGATCCCAGTCCAAATGACAATCTAT
oJW1137	ATTGGCATGCTCGACTCTCTAGCTTGAG
oJW1199	TGGTGTCAAAAATAACTCGACCTTCGATATGGGCGGATTCTT
oJW1200	GAATCCGCCCATATCGAAGGTCGAGTTATTTTTGACACCA
oJW1201	TGATGTTTGAGTCGGCTGATAGGGAAAAGGTGGTGAACTAC
oJW1202	GTAGTTCACCACCTTTTCCCTATCAGCCGACTCAAACATCAAA
oJW1203	GGCTAAGAGAACAAGGAGGAGACGGTGGAAACGAGGTCATCATTT
oJW1204	ATGACCTCGTTTCCACCGTCTCCTCCTTGTTCTCTTAGCC
oJW1213	CATAAAGGCTAGGGATAACAGGGTAATCCGCTCACAATTCCACACAAC
oJW1214	GCAGACGTTGCCATATCCAATTCAAGCTGGGGATCCTAGAAGCT
oJW1215	CTTCTAGGATCCCCAGCTTGAATTGGATATGGCAACGTCTGCCC
oJW1217	CAGAGGTTCCGATTTTAAC
oJW1218	TCAATTCAGTAACATCGTTC
oJW1221	GCTTCAGGATGATATTTACAA
oJW1222	CAGGTGTTCGATATAATCAAG
oJW1335	GTAAAACGACGGCCAGTGCGTTTCGGTGATGAAGAT
oJW1336	ATTAAAAACTGGTCTGATCGCTATGCAAGGGTTTATTGTT
oJW1337	AACAATAAACCCTTGCATAGCGATCAGACCAGTTTTTAAT
oJW1338	AGGAAATCCATTATGTACTATTTAGTACGCCTCTTTTCTTTTC
oJW1339	GAAAAGAAAAGAGGCGTACTAAATAGTACATAATGGATTTCCT
oJW1902	CCTGACTGGGAAGAGGATGACG
oJW1903	TCAGCTTTCATGGCTATCATTGAAC
oJW1904	CTGGCTGGAAATACGCTTCTCG
oJW1905	GATCAACGACGCTCAAGAGCTCA
oJW1906	GGACTGTCCGCGTCGTTACGT
oJW1907	GCTTCCTCGCTCCCTTGGG
oJW2008	GGCATGAGCCTGGGCATGTG
oJW2009	CTCCGTCTGCGTTTCGCAGTTC

b

***Bacillus* genomes**	**NCBI_accession**
Bacillus subtilis subtilis 168	NC_000964.3
Bacillus subtilis subtilis BSP1	CP003695
Bacillus subtilis QB928	CP003783.1

b

***Bacillus* genomes**	**NCBI_accession**
Bacillus subtilis 6051HGW	CP003329
Bacillus subtilis spizizenii W23	NC_014479.1
Bacillus subtilis subtilis RO-NN-1	CP002906
Bacillus subtilis spizizenii TU-B-10	NC_016047
Bacillus subtilis BSn5	NC_014976.1
Bacillus amyloliquefaciens FZB42	NC_009725.1

c

Regulator name	**Function**
AbrB	transcriptional regulator for transition state genes
AhrC	arginine repressor
AraR	transcriptional repressor of the ara regulon (LacI family)
BkdR	transcriptional regulator
CcpA	transcriptional regulator (LacI family)
CodY	transcriptional repressor CodY
ComA	two-component response regulator
ComK	competence transcription factor (CTF)
CtsR	transcriptional regulator
DegU	two-component response regulator
Fnr	transcriptional regulator (FNR/CAP family)
Fur	transcriptional regulator for iron transport and metabolism
GInR	transcriptional regulator (nitrogen metabolism)
GItC	transcriptional regulator (LysR family)
GItR	transcriptional regulator (LysR family)
Hpr	transcriptional regulator Hpr
HrcA	heat-inducible transcription repressor
IoIR	transcriptional regulator (DeoR family)
LevR	transcriptional regulator (NifA/NtrC family)
LexA	transcriptional repressor of the SOS regulon
MntR	manganese transport transcriptional regulator
Mta	transcriptional regulator (MerR family)
PerR	transcriptional regulator (Fur family)
PucR	transcriptional regulator of the purine degradation operon
PurR	pur operon repressor
ResD	two-component response regulator
RocR	transcriptional regulator (NtrC/NifA family)
SinR	transcriptional regulator for post-exponenetial-phase-response
Spo0A	master regulator of sporulation
SpoIIID	transcriptional regulator of mother cell gene expression
TnrA	nitrogen sensing transcriptional regulator
Xre	Phage PBSX transcriptional regulator
Zur	transcriptional regulator (Fur family)

Acknowledgments

We thank E. Robleto, R. Yasbin and L. Simmons for strains, M. Cox, R. Gourse, C. Hittinger, R. Landick, K. Wasserman, C. Gross, M. Laub, S. Rosenberg, L. Simmons and the Wang lab for discussions and comments on the manuscript. This work was supported by NIH Director's New Innovator Award DP2OD004433 to JDW.

References

1. French S. Consequences of replication fork movement through transcription units in vivo. Science. 1992; 258:1362–5. [PubMed: 1455232]
2. Liu B, Alberts BM. Head-on collision between a DNA replication apparatus and RNA polymerase transcription complex. Science. 1995; 267:1131–7. [PubMed: 7855590]
3. Vilette D, Ehrlich SD, Michel B. Transcription-induced deletions in Escherichia coli plasmids. Mol Microbiol. 1995; 17:493–504. [PubMed: 8559068]
4. Prado F, Aguilera A. Impairment of replication fork progression mediates RNA polII transcription-associated recombination. EMBO J. 2005; 24:1267–76. [PubMed: 15775982]
5. Mirkin EV, Mirkin SM. Mechanisms of transcription-replication collisions in bacteria. Mol Cell Biol. 2005; 25:888–895. [PubMed: 15657418]
6. Pomerantz RT, O'Donnell M. The replisome uses mRNA as a primer after colliding with RNA polymerase. Nature. 2008; 456:762–6. [PubMed: 19020502]
7. Srivatsan A, Tehranchi A, MacAlpine DM, Wang JD. Co-orientation of replication and transcription preserves genome integrity. PLoS Genet. 2010; 6:e1000810. [PubMed: 20090829]
8. Dutta D, Shatalin K, Epshtein V, Gottesman ME, Nudler E. Linking RNA polymerase backtracking to genome instability in E. coli. Cell. 2011; 146:533–43. [PubMed: 21854980]
9. Merrikh H, Machón C, Grainger WH, Grossman AD, Soultanas P. Co-directional replication-transcription conflicts lead to replication restart. Nature. 2011; 470:554–7. [PubMed: 21350489]
10. Kim N, Jinks-Robertson S. Transcription as a source of genome instability. Nat Rev Genet. 2012; 13:204–214. [PubMed: 22330764]
11. Paul S, Million-Weaver S, Chattopadhyay S, Sokurenko E, Merrikh H. Accelerated gene evolution through replication-transcription conflicts. Nature. 2013; 495:512–5. [PubMed: 23538833]
12. Fijalkowska IJ, Jonczyk P, Tkaczyk MM, Bialoskorska M, Schaaper RM. Unequal fidelity of leading strand and lagging strand DNA replication on the Escherichia coli chromosome. Proc Natl Acad Sci U S A. 1998; 95:10020–10025. [PubMed: 9707593]
13. Bruand C, Bidnenko V, Ehrlich SD. Replication mutations differentially enhance RecA-dependent and RecA-independent recombination between tandem repeats in Bacillus subtilis. Mol Microbiol. 2001; 39:1248–58. [PubMed: 11251841]
14. Hastings PJ, Lupski JR, Rosenberg SM, Ira G. Mechanisms of change in gene copy number. Nat Rev Genet. 2009; 10:551–64. [PubMed: 19597530]
15. Kunkel TA. Evolving views of DNA replication (in)fidelity. Cold Spring Harb Symp Quant Biol. 2009; 74:91–101. [PubMed: 19903750]
16. Rocha EPC, Danchin A. Essentiality, not expressiveness, drives gene-strand bias in bacteria. Nat Genet. 2003; 34:377–378. [PubMed: 12847524]
17. Reijns MAM, et al. Lagging-strand replication shapes the mutational landscape of the genome. Nature. 2015; 518:502–6. [PubMed: 25624100]
18. Schroeder JW, Hirst WG, Szewczyk GA, Simmons LA. The Effect of Local Sequence Context on Mutational Bias of Genes Encoded on the Leading and Lagging Strands. Curr Biol. 2016; 26:692–7. [PubMed: 26923786]
19. Million-Weaver S, et al. An underlying mechanism for the increased mutagenesis of lagging-strand genes in Bacillus subtilis. Proc Natl Acad Sci U S A. 2015; doi: 10.1073/pnas.1416651112
20. Luria SE, Delbrück M. Mutations of Bacteria from Virus Sensitivity to Virus Resistance. Genetics. 1943; 28:491–511. [PubMed: 17247100]
21. Rosche WA, Foster PL. Determining mutation rates in bacterial populations. Methods. 2000; 20:4–17. [PubMed: 10610800]

22. Mirkin EV, Castro Roa D, Nudler E, Mirkin SM. Transcription regulatory elements are punctuation marks for DNA replication. Proc Natl Acad Sci U S A. 2006; 103:7276–81. [PubMed: 16670199]
23. Vilette D, Uzest M, Ehrlich SD, Michel B. DNA transcription and repressor binding affect deletion formation in Escherichia coli plasmids. EMBO J. 1992; 11:3629–34. [PubMed: 1396563]
24. Tehranchi AK, et al. The transcription factor DksA prevents conflicts between DNA replication and transcription machinery. Cell. 2010; 141:595–605. [PubMed: 20478253]
25. Feklistov A, Darst Sa. Structural basis for promoter-10 element recognition by the bacterial RNA polymerase σ subunit. Cell. 2011; 147:1257–69. [PubMed: 22136875]
26. Yoshiyama K, Higuchi K, Matsumura H, Maki H. Directionality of DNA replication fork movement strongly affects the generation of spontaneous mutations in Escherichia coli. J Mol Biol. 2001; 307:1195–1206. [PubMed: 11292335]
27. Schaaper RM, Danforth BN, Glickman BW. Mechanisms of spontaneous mutagenesis: an analysis of the spectrum of spontaneous mutation in the Escherichia coli lacI gene. J Mol Biol. 1986; 189:273–84. [PubMed: 3018259]
28. Lu AL, Clark S, Modrich P. Methyl-directed repair of DNA base-pair mismatches in vitro. Proc Natl Acad Sci U S A. 1983; 80:4639–43. [PubMed: 6308634]
29. Zhang Y, et al. Structural basis of transcription initiation. Science. 2012; 338:1076–80. [PubMed: 23086998]
30. Zuo Y, Steitz TA. Crystal Structures of the E. coli Transcription Initiation Complexes with a Complete Bubble. Mol Cell. 2015; 58:534–40. [PubMed: 25866247]
31. Vasantha N, Freese E. Enzyme changes during Bacillus subtilis sporulation caused by deprivation of guanine nucleotides. J Bacteriol. 1980; 144:1119–1125. [PubMed: 6777366]
32. Janes BK, Stibitz S. Routine Markerless Gene Replacement in Bacillus anthracis. 2006; 74:1949–1953.
33. Gibson DG, et al. Enzymatic assembly of DNA molecules up to several hundred kilobases. Nat Methods. 2009; 6:343–5. [PubMed: 19363495]
34. Hall BM, Ma CX, Liang P, Singh KK. Fluctuation analysis CalculatOR: a web tool for the determination of mutation rate using Luria-Delbruck fluctuation analysis. Bioinformatics. 2009; 25:1564–5. [PubMed: 19369502]
35. Lippert MJ, et al. Role for topoisomerase 1 in transcription-associated mutagenesis in yeast. Proc Natl Acad Sci U S A. 2011; 108:698–703. [PubMed: 21177427]
36. Ter Beek A, et al. Transcriptome analysis of sorbic acid-stressed Bacillus subtilis reveals a nutrient limitation response and indicates plasma membrane remodeling. J Bacteriol. 2008; 190:1751–61. [PubMed: 18156260]
37. Sierro N, Makita Y, de Hoon M, Nakai K. DBTBS: a database of transcriptional regulation in Bacillus subtilis containing upstream intergenic conservation information. Nucleic Acids Res. 2008; 36:D93–6. [PubMed: 17962296]
38. Crooks GE, Hon G, Chandonia JM, Brenner SE. WebLogo: a sequence logo generator. Genome Res. 2004; 14:1188–90. [PubMed: 15173120]
39. Markowitz VM, et al. IMG: the Integrated Microbial Genomes database and comparative analysis system. Nucleic Acids Res. 2012; 40:D115–22. [PubMed: 22194640]
40. Gao F, Zhang CT. DoriC: a database of oriC regions in bacterial genomes. Bioinformatics. 2007; 23:1866–7. [PubMed: 17496319]
41. Katoh K, Toh H. Parallelization of the MAFFT multiple sequence alignment program. Bioinformatics. 2010; 26:1899–900. [PubMed: 20427515]
42. Suyama M, Torrents D, Bork P. PAL2NAL: robust conversion of protein sequence alignments into the corresponding codon alignments. Nucleic Acids Res. 2006; 34:W609–12. [PubMed: 16845082]
43. Guindon S, et al. New algorithms and methods to estimate maximum-likelihood phylogenies: assessing the performance of PhyML 3.0. Syst Biol. 2010; 59:307–21. [PubMed: 20525638]
44. Yang Z. PAML 4: phylogenetic analysis by maximum likelihood. Mol Biol Evol. 2007; 24:1586–91. [PubMed: 17483113]

45. Librado P, Rozas J. DnaSP v5: a software for comprehensive analysis of DNA polymorphism data. Bioinformatics. 2009; 25:1451–2. [PubMed: 19346325]

46. Lindahl T. Instability and decay of the primary structure of DNA. Nature. 1993; 362:709–15. [PubMed: 8469282]

47. Aamodt RM, Falnes PØ, Johansen RF, Seeberg E, Bjørås M. The Bacillus subtilis counterpart of the mammalian 3-methyladenine DNA glycosylase has hypoxanthine and 1,N6-ethenoadenine as preferred substrates. J Biol Chem. 2004; 279:13601–6. [PubMed: 14729667]

48. ZAMENHOF S. Gene unstabilization induced by heat and by nitrous acid. J Bacteriol. 1961; 81:111–7. [PubMed: 13787802]

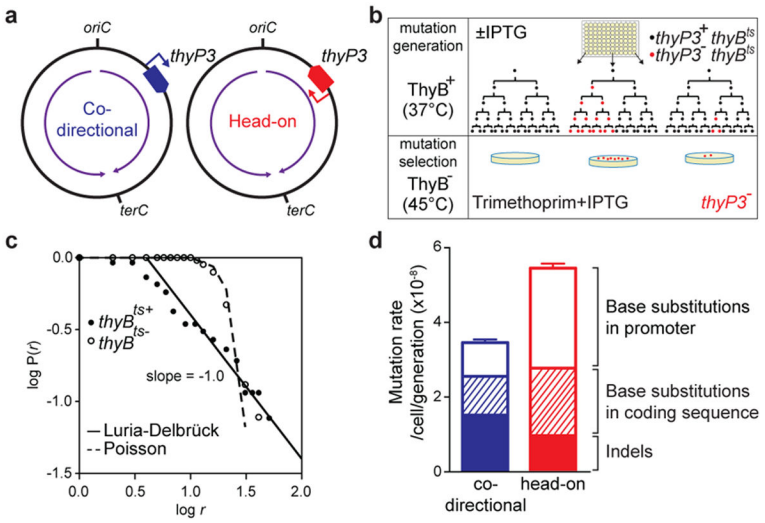

Figure 1. Transcription directionality affects spontaneous mutation rates and spectra in *B. subtilis*

a, *thyP3* gene with an IPTG-inducible promoter is integrated into the chromosome either co-directionally or head-on to replication. Purple arrow: replication direction, *oriC*: replication origin, *terC*: replication terminus. **b**, Modified fluctuation test to measure the rate of spontaneous mutations conferring trimethoprim resistance. **c**, Distribution of mutants: number of mutants per culture (*r*) plotted against proportion of cultures with ≥*r* mutants (P(*r*)). **d**, The mutation rates in co-directional and head-on *thyP3* (subdivided by mutation spectra) when transcription is induced with IPTG. Mutation rates are expressed as mean ±s.e.m here and all figures.

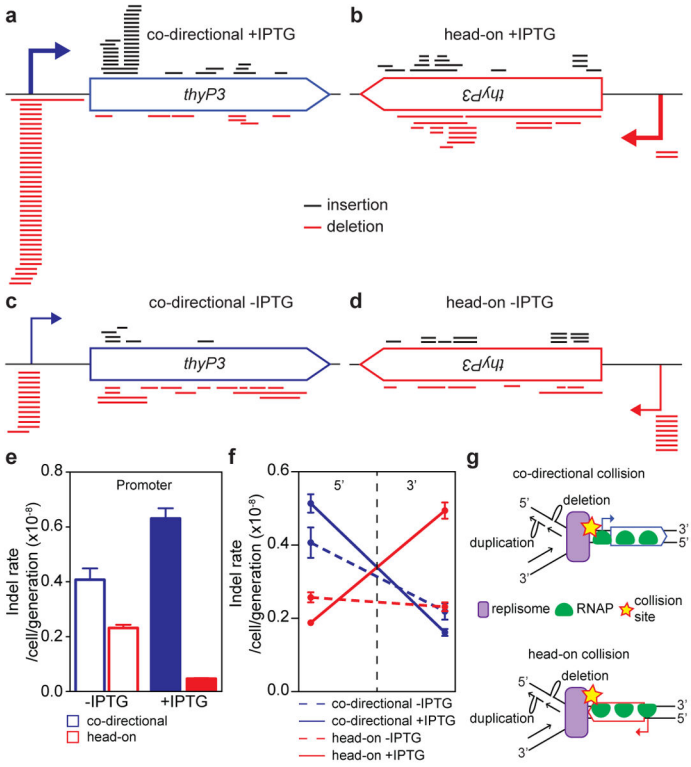

Figure 2. Distributions of indels (insertions/deletions) are strongly dependent on transcription directionality and strength

a–d, Positional distribution of indels of ≥3 bp in co-directional and head-on *thyP3* under induced (+IPTG) and un-induced (−IPTG) conditions. Each bar represents an insertion (black) or deletion (red). **e**, The rates of ≥3 bp indels at the promoter. **f,** The rates of ≥3 bp indels within 5′ (1–420 bp) and 3′ (421–840 bp) of coding region. Rates of insertions and deletions are plotted separately in Extended Data Fig. 6d. **g,** Model illustrating the mechanism of generation of indels in the vicinity of collision site in co-directional and head-on orientations, via fork slippage (shown here), template switch or fork reversal (Extended Data Fig. 6e).

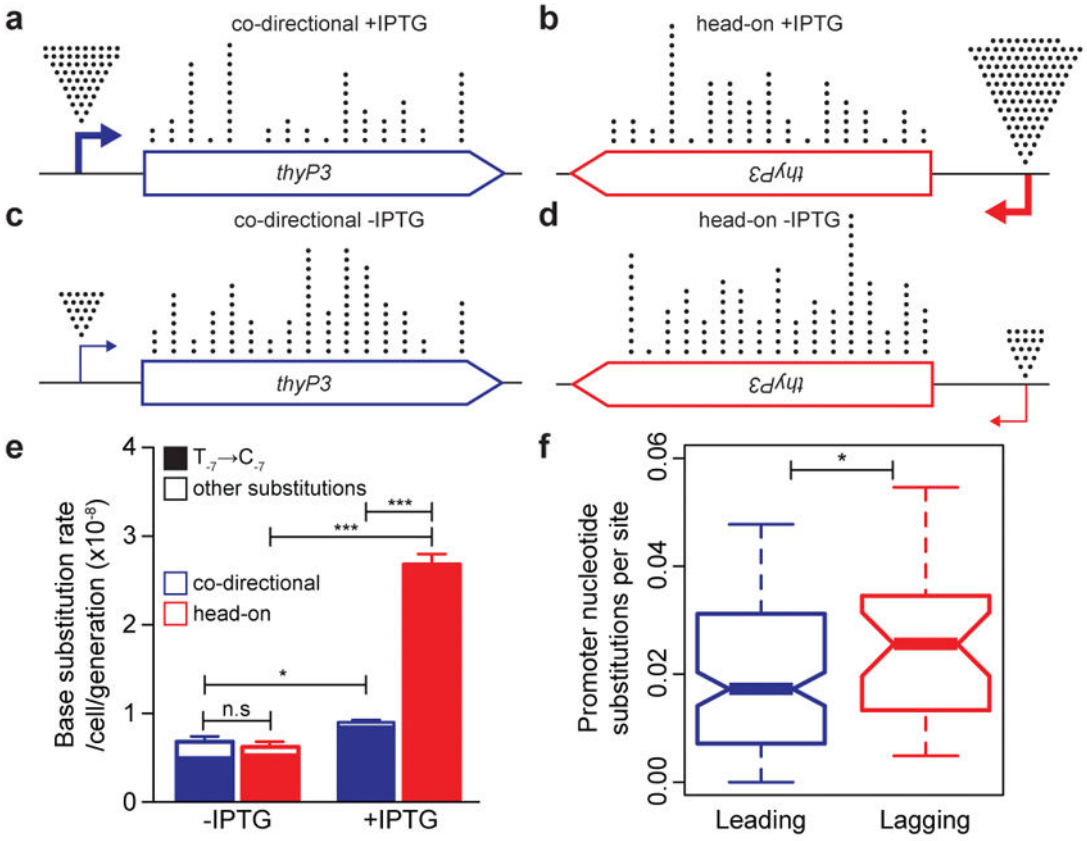

Figure 3. Head-on transcription induces base substitutions at the promoter

a–d, Positional distribution of base substitutions in co-directional and head-on *thyP3* under induced (+IPTG) and un-induced (−IPTG) conditions. Each dot records a base substitution mapped in 50 nt window. **e**, Promoter base substitution rate is strongly increased in head-on orientation upon IPTG-induction. **f-,** Distribution of mean nucleotide substitutions per site of promoters, each estimated pairwise among *Bacillus* strains. Lagging strand promoters (n=32) show increased substitutions than leading strand promoters (n=147). Nucleotide substitutions are comparable between promoters bound and not bound by transcriptional repressors (Extended Data Fig. 8c). Central mark of box-plot represents median, edges are 25th and 75th centiles, notches are 95% CI of median, and whiskers represent extreme data points within range. (n.s-not significant; *P<0.05, **P<0.01, ***P<0.0001; Student's *t*-test, Mann-Whitney U test).

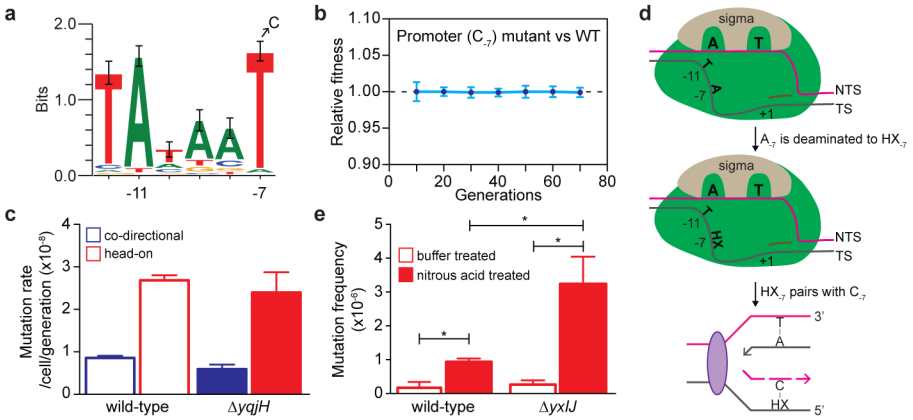

Figure 4. Promoter T$_{-7}$→C$_{-7}$ is a mutation hotspot generated via deamination

a, The consensus −10 element of *B. subtilis* SigA-dependent promoters (n=358). The strongly conserved T$_{-7}$ is frequently mutated to a C. **b**, Fitness of head-on T$_{-7}$→C$_{-7}$ mutant relative to head-on wild-type *thyP3* cells under induced transcription (mean±s.d). **c**, Mutation rate of T$_{-7}$→C$_{-7}$ in *yqjH* mutant (error-prone polymerase PolIV). **d**, Model illustrating the mechanism of generation of T$_{-7}$→C$_{-7}$. During transcription initiation, the −10 element is single-stranded, creating solvent accessibility for A$_{-7}$ on the template strand (TS), allowing it to be deaminated to hypoxanthine (HX). HX basepairs with C during replication, resulting in T$_{-7}$→C$_{-7}$. **e**, T$_{-7}$→C$_{-7}$ frequencies in head-on *thyP3* upon nitrous acid treatment of wild-type and Δ*yxlJ* (hypoxanthine-DNA glycosylase) strains. (*-P<0.05; Student's *t*-test).